

Bahadir K. Gunturk, John Glotzbach, Yucel Altunbasak,
Ronald W. Schafer, and Russel M. Mersereau



Demosaicking: Color Filter Array Interpolation

Exploring the imaging process and the correlations among three color planes in single-chip digital cameras

Digital cameras have become popular, and many people are choosing to take their pictures with digital cameras instead of film cameras. When a digital image is recorded, the camera needs to perform a significant amount of processing to provide the user with a viewable image. This processing includes correction for sensor nonlinearities and nonuniformities, white balance adjustment, compression, and more. An important part of this image processing chain is color filter array (CFA) interpolation or demosaicking.

A color image requires at least three color samples at each pixel location. Computer images often use red (R), green (G), and blue (B). A camera would need three separate sensors to completely measure the image. In a three-chip color camera, the light entering the camera is split and projected onto each spectral sensor. Each sensor requires its proper driving electronics, and the sensors have to be registered precisely. These additional requirements add a large expense to the system. Thus, many cameras use a single sensor covered with a CFA. The CFA allows only one color to be measured at each pixel. This means that the camera must estimate the missing two color values at each pixel. This estimation process is known as demosaicking.

Several patterns exist for the filter array. The most common array is the Bayer CFA, shown in Figure 1. The Bayer array measures the G image on a quincunx grid and the R and B images on rectangular grids. The G image is measured at a higher sampling rate because the peak sensitivity of the human visual system lies in the medium wavelengths, corresponding to the G portion of the spec-

trum. Other patterns are also used, e.g., the Nikon Coolpix 990 uses a cyan, magenta, yellow, G (CMYG) grid, where each of the four images are sampled using rectangular grids. A CMY-based system has the advantage of being more sensitive to light because the incoming light only has to pass through one layer of filters. RGB filters are generated by overlaying combinations of CMY filters [2]. For example, the combination of CM filters would make a B filter. Even though other options exist, this article discusses the demosaicking problem with reference to the Bayer RGB CFA.

If the measured image is divided by measured color into three separate images, this problem looks like a typical image interpolation problem. Therefore, one might try to apply standard image interpolation techniques. Bicubic interpolation is a common image interpolation technique that produces good interpolation results when applied to grayscale images. However, when bicubic interpolation is used for this problem, the resulting image shows many visible artifacts. This is illustrated in Figure 2.

This result motivates the need to find a specialized algorithm for the demosaicking problem. Bicubic interpolation and other standard interpolation techniques treat the color image as three independent images. However, the three images are generally highly correlated. Many algorithms have been published suggesting how to use this correlation. This article surveys many of these algorithms and discusses the results in terms of objective and subjective measures.

IMAGE FORMATION PROCESS

Since some of the demosaicking methods make explicit use of image formation models, we provide a brief summary of image formation before reviewing the demosaicking methods. The imaging process is usually modeled as a linear process between the light radiance arriving at the camera and the pixel intensities produced by the sensors. Most digital cameras use charge-coupled device (CCD) sensors. In a CCD camera, there is a rectangular grid of electron-collection sites laid over a silicon wafer to record the amount of light energy reaching each of them. When photons strike these sensor sites, electron-hole pairs are generated, and the electrons generated at each site are collected over a certain period of time. The numbers of electrons are eventually converted to pixel values.

Each sensor type, S , has a specific spectral response $L_S(\lambda)$, which is a function of the spectral wavelength λ , and a spatial response $h_S(x, y)$, which results from optical blur and spatial integration at each sensor site. In practice, discrete formulation of the imaging process is used

$$S(n_1, n_2) = \sum_l \sum_{m_1, m_2} L_S(l) h_S(n_1 - m_1, n_2 - m_2) \times r(m_1, m_2, l) + N_S(n_1, n_2). \quad (1)$$

where $S(n_1, n_2)$ is the intensity at spatial location (n_1, n_2) , $r(m_1, m_2, l)$ is the incident radiance, and $N_S(n_1, n_2)$ is the addi-

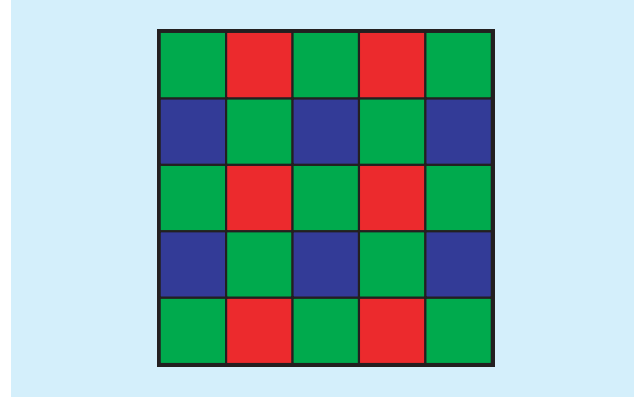


[FIG1] Bayer color filter array arrangement.

tive noise that is a result of thermal/quantum effects and quantization. There are a couple of assumptions in this formulation: 1) the input-output relationship is assumed to be linear, 2) the spatial blur $h_S(n_1, n_2)$ is assumed to be space-invariant and independent of wavelength, and 3) only the additive noise is considered. These assumptions are reasonable for practical purposes.

The last step in the imaging process is the CFA sampling. Denoting Λ_S as the set of pixel locations, (n_1, n_2) , for channel S , a CFA mask function can be defined as

$$f_S(n_1, n_2) = \begin{cases} 1, & (n_1, n_2) \in \Lambda_S \\ 0, & \text{otherwise} \end{cases}. \quad (2)$$

In the Bayer CFA, there are three types of color channels: R, G, and B. Therefore, for the Bayer CFA, the observed data, $O(n_1, n_2)$, is

$$O(n_1, n_2) = \sum_{S=R,G,B} f_S(n_1, n_2) S(n_1, n_2). \quad (3)$$

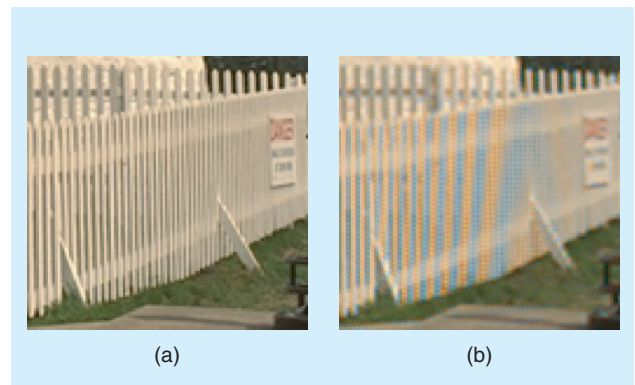
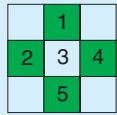


[FIG2] Bicubic interpolation used for color filter array interpolation results in noticeable artifacts: (a) original image and (b) bicubic interpolation.



1. Calculate horizontal gradient $\Delta H = |G2 - G4|$
2. Calculate vertical gradient $\Delta V = |G1 - G5|$
3. If $\Delta H > \Delta V$,
 $G3 = (G1 + G5)/2$
 Else if $\Delta H < \Delta V$,
 $G3 = (G2 + G4)/2$
 Else
 $G3 = (G1 + G5 + G2 + G4)/4$

[FIG3] Edge-directed interpolation for the G channel is illustrated. G1, G2, G4, and G5 are measured G values; G3 is the estimated G value at pixel 3.

DEMOSAICKING METHODS

We examine demosaicking methods in three groups. The first group consists of heuristic approaches. The second group formulates demosaicking as a restoration problem. The third group is a generalization that uses the spectral filtering model given in (1).

HEURISTIC APPROACHES

Heuristic approaches do not try to solve a mathematically defined optimization problem. They are mostly filtering operations that are based on reasonable assumptions about color images. Heuristic approaches may be spatially adaptive, and they may exploit correlation among the color channels. We now overview these heuristic approaches.

EDGE-DIRECTED INTERPOLATION

Although nonadaptive algorithms (e.g., bilinear interpolation or bicubic interpolation) can provide satisfactory results in smooth regions of an image, they usually fail in textured regions and edges. Edge-directed interpolation is an adaptive approach, where the area around each pixel is analyzed to determine if a preferred interpolation direction exists. In practice, the interpolation direction is chosen to avoid interpolating across edges, instead interpolating along any edges in the image.

An illustration of edge-directed interpolation is shown in Figure 3, where horizontal and vertical gradients at the location where G is not measured are calculated from the adjacent G pixels.

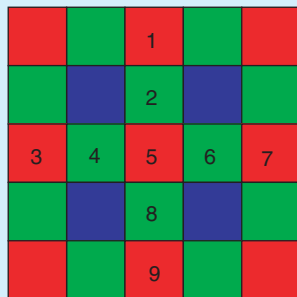
els. In [17], these gradients are compared to a constant threshold. If the gradient in one direction falls below the threshold, interpolation is performed only along this direction. If both gradients are below or above the threshold, the pixels along both directions are used to estimate the missing value.

The edge-directed interpolation idea can be modified by using larger regions (around the pixel in question) with more complex predictors and by exploiting the texture similarity in different color channels. In [23], the R and B channels (in the 5×5 neighborhood of the missing pixel) are used instead of the G channel to determine the gradients. To determine the horizontal and vertical gradients at a B (R) sample, second-order derivatives of B (R) values are used. This algorithm is illustrated in Figure 4. Another example of the edge-directed interpolation is found in [19], where the Jacobian of the R, G, and B samples is used to determine edge directions.

CONSTANT-HUE-BASED INTERPOLATION

One commonly used assumption in demosaicking is that the hue (color ratios) within an object in an image is constant. In [22], it is explained that an object of constant color will have a constant color ratio even though lighting variations may change the measured values. This perfect interchannel correlation assumption is formulated such that the color differences (or color ratios or logarithm of color ratios) within objects are constant. This constant color difference (or ratio) assumption prevents abrupt changes in hue and has been extensively used for the interpolation of the R and B channels [9], [34], [3], [23], [17], [10], [22], [30], [27].

As a first step, these algorithms interpolate the G channel, which is done using bilinear or edge-directed interpolation. The R and B channels are then estimated from the interpolated R hue (R-to-G ratio) and B hue (B-to-G ratio). To be more explicit, the interpolated R hue and B hue values are multiplied by the G value to determine the missing R and B values at a particular pixel location. The color ratios can be interpolated with any method (bilinear, bicubic, or edge directed). Instead of interpolating the color ratios, the color differences can also be interpolated, as described in Figure 5.



1. Calculate horizontal gradient $\Delta H = |(R3 + R7)/2 - R5|$
2. Calculate vertical gradient $\Delta V = |(R1 + R9)/2 - R5|$
3. If $\Delta H > \Delta V$,
 $G5 = (G2 + G8)/2$
 Else if $\Delta H < \Delta V$,
 $G5 = (G4 + G6)/2$
 Else
 $G5 = (G2 + G8 + G4 + G6)/4$

[FIG4] Edge-directed interpolation in [23] is illustrated for estimating the G value at pixel 5. The R values are used to determine the edge direction. When the missing G value is at a B pixel, the B values are used to determine the edge direction.

WEIGHTED AVERAGE

In edge-directed interpolation, the edge direction is estimated first, and then the missing sample is estimated by interpolating along the edge. Instead, the likelihood of an edge in a certain direction can be found, and the interpolation can be done based on the edge likelihoods. Such an algorithm was proposed by Kimmel in [22]. The algorithm defines edge indicators in several directions as measures of edge likelihood in those directions and determines a missing pixel

intensity as a weighted sum of its neighbors. If the likelihood of an edge crossing in a particular direction is high, the edge indicator returns a small value, which results in less contribution from the neighboring pixel in that direction. The G channel is interpolated first; the R and B channels are interpolated from the R-to-G and B-to-G ratios. The color channels are then updated iteratively to obey the constant color ratio rule.

A similar algorithm was proposed recently in [25], where edge indicators are determined in a 7×7 window for the G and a 5×5 window for the R and B channels. In this case, the edge indicator function is based on the L_1 norm (absolute difference) as opposed to the L_2 norm of [22]. A related algorithm is proposed in [35], where the directions (horizontal, vertical, diagonal) that have the smallest two gradients are used in interpolation.

A different example of weighted directional interpolation can be found in [33], where fuzzy membership assignment is used to compute weights for the horizontal and vertical direction. The weights are computed experimentally and used as constants in the algorithm. In [28], a bilateral filter kernel is generated at each pixel to enforce similarity within a neighborhood. This filtering approach is adaptive and allows for noise reduction and sharpening of edges.

SECOND-ORDER GRADIENTS AS CORRECTION TERMS

In [4], Hamilton and Adams begin by using edge-directed interpolation for the G image. Correction terms from the R and B samples are added to this initial estimate. They compute the Laplacian for the R or B samples along the interpolation row or column and use this to correct the simple averaging interpolation. This correction term reduces aliasing passed to the output by the simple averaging filter. Figure 6 illustrates this algorithm.

ALIAS CANCELING INTERPOLATION

In [12], the G image is used to add high-frequency information and reduce aliasing in the R and B images. First, the R and B images are interpolated with a rectangular low-pass filter according to the rectangular sampling grid. This fills in the missing values in the grid but allows aliasing distortions into the R and B output images. These output images are also missing the high-frequency components needed to produce a

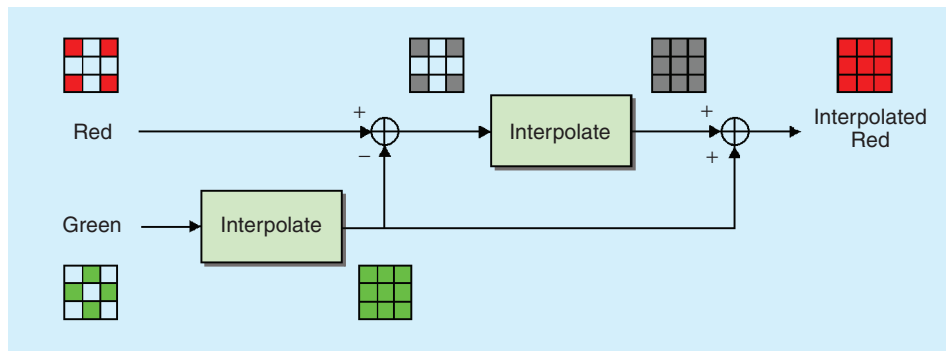


[FIG5] Constant-difference-based interpolation is illustrated for the R channel. The B channel is interpolated similarly.

sharp image. However, because the G image is sampled at a higher rate, the high-frequency information can be taken from the G image to improve an initial interpolation of the R and B images. A horizontal high-pass filter and a vertical high-pass filter are applied to the G image. This provides the high-frequency information that the low sampling rate of the R and B images cannot preserve. Aliasing occurs when high-frequency components are shifted into the low-frequency portion of the spectrum, so if the outputs of the high-pass filters are modulated into the low-frequency regions, an estimate of the aliasing in the R and B images can be found. This estimate is used to reduce the aliasing in the R and B images, as illustrated in Figure 7. This method relies on the assumption that the high-frequency information in the R, G, and B images is identical. If this assumption does not hold, the addition of the G information into the R and B images can add unwanted distortions. This method also makes the assumption that the input image is band-limited within the diamond-shaped Nyquist region of the G quincunx sampling grid. When this assumption fails, the aliasing artifacts are enhanced instead of reduced, because the G image also contains aliasing.

HOMOGENEITY-DIRECTED INTERPOLATION

Instead of choosing the interpolation direction based on edge indicators, it is possible to use different measures. In [18], local

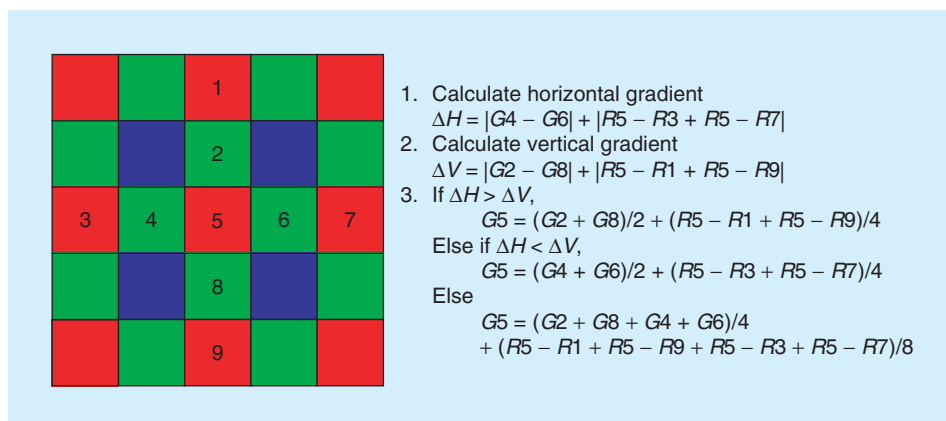


[FIG6] The Hamilton and Adams method [4] is illustrated for estimating the G value at pixel 5. The R and G values are used to determine the edge direction and estimate the missing value. When the missing G value is at a B pixel, the B and G values are used.

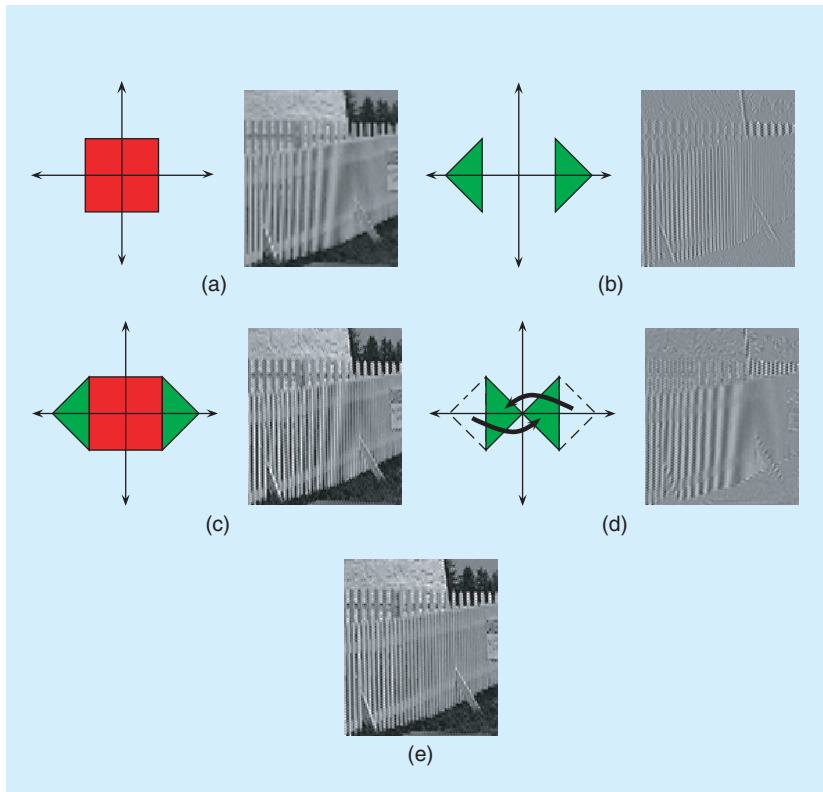


[FIG7] High-frequency information from the green image is modulated and used to cancel aliasing in the red image: (a) low-pass filter of the sampled red image, (b) isolated high-frequency components in the green image, (c) aliasing estimate subtracted from the red image, (d) green high-frequency components modulated to estimate aliasing in the red image, and (e) aliasing estimate subtracted from the red image.

homogeneity is used as an indicator to choose between horizontally and vertically interpolated intensities. The homogeneity-directed interpolation imposes the similarity of the luminance and chrominance values within small neighborhoods. The RGB data is first interpolated horizontally and vertically, i.e., there are two candidates for each missing color sample. The decision for which one to choose is made in the CIELAB space, a perceptually uniform color space. Both the horizontally and vertically interpolated images are transformed to the CIELAB space. In the CIELAB space, either the horizontally or the vertically interpolated pixel values are chosen based on the local homogeneity. The local homogeneity is measured by the total number of similar luminance and chrominance values of the pixels that are within a neighborhood of the pixel in question. Two values are taken as similar when the Euclidean distance between them is less than a threshold.

PATTERN MATCHING

Several algorithms attempt to find a pattern in the data or fit the data to one of several templates. A different interpolator is applied for each template. This allows different methods to be used for edges and smooth regions. In [9], Cok describes a pattern matching algorithm to be used on the G image. Each missing G value is classified as a stripe, edge, or

corner, corresponding to the features expected to be found in natural images. After classifying the pixel, an appropriate interpolator is applied to estimate the missing value.

In [8], Chang et al. introduce a method using directional information and add the ability to use multiple directions. This method uses eight possible horizontal, vertical, and diagonal interpolation directions. A gradient is computed for each direction, and then a threshold is computed based on these gradients to determine which directions are used. For each direction included in the interpolation, an average R, G, and B value is computed. For each of the missing colors at the current pixel, the difference between the average of the missing color and the average of the color of the current pixel is calculated. This color difference is added to the value of the current pixel to estimate the missing color value.

VECTOR-BASED INTERPOLATION

In this approach, each pixel is considered as a vector in the three-dimensional (R, G, B) space, and interpolation is designed to minimize the angle or the distance among the neighboring vectors. One of the algorithms proposed in [21] is based on the minimization of angles in spherical coordinates. After

an initial interpolation of missing samples, each pixel is transformed to spherical coordinates, (ρ, θ, ϕ) . The relationship between the (R, G, B) space and (ρ, θ, ϕ) space is

$$R = \rho \cos(\theta) \sin(\phi); \quad G = \rho \cos(\theta) \cos(\phi);$$

$$\text{and } B = \rho \sin(\theta). \quad (4)$$

In the (ρ, θ, ϕ) space, some filtering operation, such as median filtering, is applied to the angles θ and ϕ only. This forces the chrominance components to be similar. Because ρ is closely related to the luminance component, keeping it unchanged preserves the luminance discontinuities among neighboring pixels. After the filtering process, the image is transformed back to the (R, G, B) space, and original measured samples are inserted into their corresponding locations. Spherical domain filtering and insertion operations are repeated iteratively.

Another vector-based interpolation is proposed in [15]. In contrast to the approach in [21], the RGB vectors are constructed from observed data only. All possible R, G, and B combinations in a 3×3 neighborhood of a pixel are used to form the so-called pseudopixels. The colors at the center of the 3×3 region are found from the vector median of the pseudopixels. The formation of pseudopixels is illustrated in Figure 8. The vector median (VM) operation is defined as

$$\begin{bmatrix} x_1 \\ x_2 \\ x_3 \end{bmatrix} = VM \left\{ \begin{bmatrix} v_{11} \\ v_{12} \\ v_{13} \end{bmatrix}, \begin{bmatrix} v_{21} \\ v_{22} \\ v_{23} \end{bmatrix}, \dots, \begin{bmatrix} v_{N1} \\ v_{N2} \\ v_{N3} \end{bmatrix} \right\} \\ \equiv \arg \min_{x_1, x_2, x_3} \sum_{i=1}^N \left(\sum_{k=1}^3 (x_k - v_{ik})^2 \right)^{1/2}. \quad (5)$$

There is no closed-form solution to (5); the vector median can be found iteratively by some numerical methods [15]. Note that the reconstructed color channels are not necessarily consistent with the observed data. It is argued that this would reduce color artifacts even if the edge locations are shifted in the end.

FOURIER-DOMAIN FILTERING

In [5], it is shown that CFA samples can be written as a summation of luminance and chrominance terms, which are well localized in frequency domain. Therefore, the luminance and chrominance terms can be recovered by low-pass and high-pass filtering. The formulation starts with the representation of CFA data, $O(n_1, n_2)$, in terms of R, G, and B channels

$$O(n_1, n_2) = \sum_{S=R,G,B} m_S(n_1, n_2) S(n_1, n_2), \quad (6)$$

where $m_S(n_1, n_2)$ are the modulation functions defined as

$$m_R(n_1, n_2) = (1 + \cos(\pi n_1)) (1 + \cos(\pi n_2)) / 4, \quad (7)$$

$$m_G(n_1, n_2) = (1 - \cos(\pi n_1) \cos(\pi n_2)) / 2, \quad (8)$$

$$m_B(n_1, n_2) = (1 - \cos(\pi n_1)) (1 - \cos(\pi n_2)) / 4. \quad (9)$$

The modulation functions can be written as a summation of a constant term and a sinusoidal term $\tilde{m}_S(n_1, n_2)$. Therefore, (6) can be written as

$$O(n_1, n_2) = \frac{1}{4} (R(n_1, n_2) + 2G(n_1, n_2) + B(n_1, n_2)) \\ + \sum_{S=R,G,B} \tilde{m}_S(n_1, n_2) S(n_1, n_2). \quad (10)$$

The first term in (10) is called as the luminance term because it does not depend on the sinusoids; the second term is called the chrominance term. In the Fourier domain, the luminance terms are located in the low-frequency regions, while the chrominance terms are located in the high-frequency regions. Although there may be some spectral overlap, the luminance and chrominance

can be estimated by low-pass filtering and high-pass filtering, respectively. R, G, and B samples are then found from the luminance and chrominance terms.

RECONSTRUCTION APPROACHES

The second group of algorithms makes some assumptions about the interchannel correlation or the prior image and solves a mathematical problem based on those assumptions. One of the methods proposed in [21] uses spatial smoothness and color correlation terms in a cost function that is minimized iteratively. In [14], an iterative algorithm that forces similar high-frequency components among the color channels

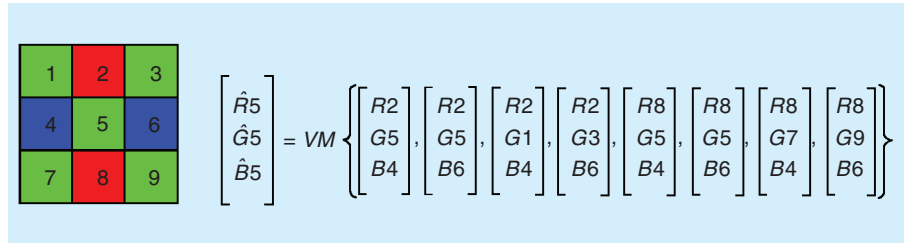


[FIG8] The formation of pseudopixels in [15] is shown. Vector median (VM) operation is applied to the pseudo-pixels to estimate the colors at pixel 5.

and ensures data consistency is proposed. In [26], the demosaicking problem is formulated as a Bayesian estimation problem, where spatial smoothness and constant hue assumptions are used as regularization terms.

REGULARIZATION

In [21], Keren and Osadchy propose a regularization approach, which minimizes a cost function consisting of a spatial smoothness and a color correlation term. To write the cost function, we first define vector $V(n_1, n_2)$ as

$$V(n_1, n_2) = [R(n_1, n_2) - \bar{R}, G(n_1, n_2) - \bar{G}, B(n_1, n_2) - \bar{B}]^T, \quad (11)$$

where \bar{R} , \bar{G} , and \bar{B} are the average colors in the vicinity of the pixel at (n_1, n_2) . Denoting $C_{n_1 n_2}$ as the covariance matrix of the RGB values, and $S_{n_1 n_1}$, $S_{n_1 n_2}$, and $S_{n_2 n_2}$ as the spatial derivatives in the horizontal, diagonal, and vertical direction, respectively, the cost function is defined as

$$\text{Cost} = \int \int \sum_{S=R,G,B} (S_{n_1 n_1}^2 + 2S_{n_1 n_2}^2 + S_{n_2 n_2}^2) dn_1 dn_2 \\ + \lambda \int \int V(n_1, n_2)^T C_{n_1 n_2}^{-1} V(n_1, n_2) dn_1 dn_2, \quad (12)$$

where λ is a positive constant. Restoration is achieved by minimizing this cost function iteratively. The algorithm starts with an initial interpolation of the missing values, estimates the local averages and covariance matrix based on the current values, and

minimizes the cost function using a finite-element method. In another version of the algorithm, the second term in (12) is replaced by the summation of the squared norms of the vector products of neighboring pixels. Since the vector product gives sine of the angle between two vectors, this term tries to minimize the angle among neighboring pixels.

PROJECTIONS ONTO CONVEX SETS APPROACH

In [14], Gunturk et al. propose an algorithm that forces similar high-frequency characteristics for the R, G, and B channels and ensures that the resulting image is consistent with the observed data. The algorithm defines two constraint sets, and reconstructs the color channels using the projections onto convex sets (POCS) technique. The “observation” constraint set ensures that the interpolated color channels are consistent with the observed data. That is, the color samples captured by the digital camera are not changed during the reconstruction process. The “detail” constraint set imposes similar high-frequency components in the color channels. The formal definition of the “detail” constraint set is based on the subband decomposition of the color channels: The absolute difference between the detail subbands of the R (B) channel and the G channel is constrained to be less than a threshold at each spatial location. These two constraint sets are shown to be convex in [14]. According to the algorithm, the color channels are first interpolated to get the initial estimates. R and B channels are then updated by projection onto the “detail” constraint set and the “observation” constraint set iteratively. Projection onto the “detail” constraint set is performed by 1) decomposing the color channels into frequency subbands with a bank of analysis filters, 2) updating the detail subbands of the R and B channels so that they are within a threshold distance to the detail subbands of the G channel, and 3) restoring them with a bank of synthesis filters. Projection onto the “observation” constraint set is performed by inserting the observed data into their corresponding locations in the color channels.

BAYESIAN APPROACH

With the Bayesian estimation approach, it is possible to incorporate prior knowledge about the solution (such as spatial smoothness and constant color ratio) and the noise statistics into the solution. In the maximum a posteriori probability (MAP) formulation, the observed data $O(n_1, n_2)$, the full color channels $S(n_1, n_2)$, and the additive noise $N_S(n_1, n_2)$ are all assumed to be random variables. Denoting $p(S|O)$ as the conditional probability density function (PDF), the MAP estimate \hat{S} is given by

$$\hat{S} = \arg \max_S \{p(S|O)\} = \arg \max_S \{p(O|S) p(S)\}. \quad (13)$$

To find the MAP estimate \hat{S} , the conditional PDF, $p(O|S)$, and the prior PDF, $p(S)$, need to be modeled. The conditional PDF, $p(O|S)$, is derived from the noise statistics, which is usually

assumed to be white Gaussian. As for the prior PDF, different models have been proposed.

In [26] and [16], Markov random field (MRF) models were used. In MRF processing, the conditional and prior PDFs can be modeled as Gibbs distributions. The Gibbs distribution has an exponential form, and it is characterized by an energy function and a temperature parameter. A PDF with Gibbs distribution can be written as

$$p(x) = \frac{1}{Z} e^{-U(x)/T}, \quad (14)$$

where $U(\cdot)$ is the energy function, T is the temperature parameter, and Z is the normalization constant. One feature of the MRF is that the total energy function U can be written as a sum of local energy functions, which allows for localized reconstruction [11]. In [26], three types of local energy functions are defined at each pixel location. The first energy function is associated with the additive noise, the second energy function imposes spatial smoothness, and the third energy function imposes constancy of cross color ratios. Once the local energy functions are defined, the solution minimizing the total energy can be found using a variety of techniques. In [26], simulated annealing technique was used.

As an alternative, [16] proposes a prior based on the steerable wavelet decomposition. With the steerable wavelet decomposition, images can be represented as a sum of band-pass components, each of which can be decomposed into a set of oriented bands using steerable filters. Such a directional decomposition enables imposing edge-oriented smoothness instead of an isotropic smoothness. Therefore, across-the-edge averaging is avoided. Directional energy functions are defined at different scales of a Laplacian pyramid, and a gradient descent procedure is applied to find the image that minimizes the energy functions at all scales.

During digital image acquisition, a compression process is likely to follow the interpolation process. A Bayesian approach where the distribution of the compression coefficients is modeled and used in reconstruction is proposed in [6].

ARTIFICIAL NEURAL NETWORK APPROACH

Demosaicking is an under-determined problem. Assumptions such as spatial smoothness and constant hue are used to regularize it. Obviously, these assumptions are not necessarily correct for all cases. The use of artificial neural networks (ANNs) is an alternative approach. The ANN approach uses training images to learn the parameters to be used in reconstruction. In [20], three methods based on ANNs are proposed: perceptron, backpropagation, and quadratic perceptron. In all these methods, images are processed in 2×2 neighborhoods. To have more information about the local characteristics, pixels around the 2×2 neighborhoods are also used as inputs. That is, 16 inputs are supplied to the network and eight outputs (two missing values in each 2×2 neighborhood) are estimated. In the perceptron method, the outputs are linear combina-

tions of the inputs. The weights are learned from training data. It turns out that the perceptron network is not satisfactory in high-frequency regions of the image. The backpropagation network is capable of learning complex nonlinear functions, and produces better results in the high-frequency regions than the perceptron network. On the other hand, the backpropagation network fails in the low frequency regions due to the non-linearity of the sigmoid function. To solve this problem, Kapah and Hel-Or proposes a selector, which is also an ANN, to select either the output of the perceptron network or the backpropagation network in each 2×2 neighborhood. The last method is the quadratic perceptron network. In contrast to the perceptron network, the weights are not fixed, but functions of inputs. An additional perceptron subnetwork is used to produce the weights. The overall performance of the quadratic perceptron network is reported to be the best in [20]. Another algorithm based on ANN is proposed in [13], where a three-layer feedforward structure is used. For each color channel, 16 measured pixels around a missing pixel are used as the input.

IMAGE FORMATION MODELING

The last group of methods uses a model of the image formation process and formulates the demosaicking problem as an inverse problem. These algorithms account for the transformations performed by the color filters, lens distortions, and sensor noise and determine the most likely output image given the measured CFA image. Referring to (1) and (3), the purpose is to reconstruct the radiance $r(m_1, m_2, l)$. Defining \mathbf{r} , \mathbf{O} , and \mathbf{N} as the stacked forms of $r(m_1, m_2, l)$, $O(n_1, n_2)$, and $N_S(n_1, n_2)$, respectively, the observation model can be written in the compact form

$$\mathbf{O} = \mathbf{H}\mathbf{r} + \mathbf{N}, \quad (15)$$

where \mathbf{H} is the matrix that includes the combined effects of optical blur, sensor blur, spectral response, and CFA sampling. In [31], [32], and [7] the minimum mean square error (MMSE) solution is given:

$$\hat{\mathbf{r}} = E[\mathbf{r}\mathbf{O}^T] \left(E[\mathbf{O}\mathbf{O}^T] \right)^{-1} \mathbf{O}, \quad (16)$$

where $E[\cdot]$ is the expectation operation. In [7], the point spread function is taken as an impulse function, and \mathbf{r} is represented as a weighted sum of spectral basis functions to reduce the dimensionality of the problem. (Results with nonimpulse point spread function are provided in [24].) In [32], adaptive reconstruction and ways to reduce computational complexity

are discussed. In [31], a finite-support filter is derived based on the assumption that the radiance, \mathbf{r} , is independent of scale at which the image is formed.

COMPARISON

Some of the algorithms we discussed are compared here with objective measures [mean square error (MSE)] and subjective image quality. Image results from each of the algorithms are provided. For these experiments, simulated sampling was used where full-color images were sampled to match the CFA sampling process.

Twenty-four digital color images were used in the objective measure experiments. These images are part of the Kodak color image database and include various scenes. The images were

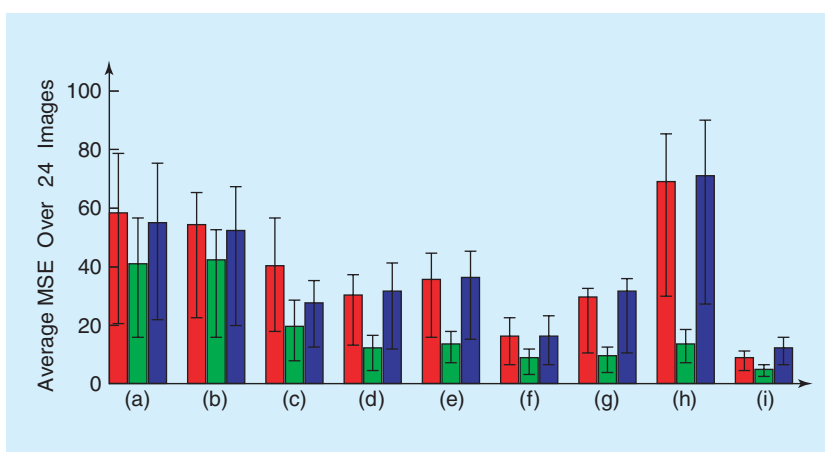


FIG9 The average mean square error for different algorithms. (a) Edge-directed interpolation in [17]. (b) Constant-hue-based interpolation in [3]. (c) Weighted sum in [22]. (d) Second-order gradients as correction terms in [4]. (e) Bayesian approach in [26]. (f) Homogeneity-directed in [18]. (g) Pattern matching in [8]. (h) Alias cancellation in [12]. (i) POCS in [14].

TABLE 1 COMPARISON WITH RESPECT TO THE CIELAB AND ZIPPER EFFECT MEASURES. REPORTED IS THE AVERAGE ERROR OVER 24 IMAGES AND THE INTERQUARTILE RANGE (IQR).

ALGORITHM	ΔE_S		ZIPPER EFFECT	
	MEAN	IQR	MEAN	IQR
(A)	2.1170	0.9444	0.2383	0.1519
(B)	1.6789	0.7599	0.2501	0.1628
(C)	2.0455	0.7647	0.0718	0.0208
(D)	1.4106	0.5539	0.2114	0.1291
(E)	1.3544	0.6980	0.2449	0.1716
(F)	0.9751	0.5960	0.0509	0.0406
(G)	1.3908	0.5644	0.1244	0.0692
(H)	1.6030	0.6681	0.4484	0.2186
(I)	0.9688	0.4619	0.0566	0.0488

(a) Edge-directed interpolation in [17]. (b) Constant-hue-based interpolation in [3]. (c) Weighted sum in [22]. (d) Second-order gradients as correction terms in [4]. (e) Bayesian approach in [26]. (f) Homogeneity-directed in [18]. (g) Pattern matching in [8]. (h) Alias cancellation in [12]. (i) POCS in [14].

sampled according to the Bayer CFA and reconstructed with a subset of the algorithms. Three measures were used to evaluate the algorithms. The MSE was measured for each color plane on each of the output images to determine the difference between the original image and the reconstructed image. For a second measure, an extension of the CIELAB measure was used. The extension, ΔE_s , is described in [36], and a MATLAB code example is available online [1]. It measures error in a perceptually uniform color space, extending the CIELAB measure to account for nonuniform regions. A third measure used in the evaluation is a measure of zipper effect [25]. Zipper effect is defined in the article as “an increase in color difference with respect to its most similar neighbor.” To determine if a pixel is affected by zipper effect, Lu and Tan compare the color change between neighboring pixels in the original, full-color image and the demosaicked image. The original image is used to determine the most similar neighbor. If the color change exceeds a fixed threshold, that pixel is determined to have zipper effect. The error measure reports the percentage of pixels that have zipper effect.

The bar graph in Figure 9 shows the average MSE over the set of images, along with error bars showing the 25–75% range for the set of images. The graph shows that the POCS method performs best on average in terms of MSE, and the small range

shown in the graph shows that it is also robust and performs well for all of the images.

Table 1 reports the ΔE_s error and the percentage of pixels showing zipper effect. The errors are reported for the same set of algorithms. These measures agree with the MSE comparison. The POCS method and the homogeneity-directed algorithm show superior results to the other algorithms.

The numbers can only provide part of the overall story. An important evaluation is the subjective appearance of the output images. For this, two example images are presented. Figure 10 shows the “lighthouse” image. This example includes a picket fence from a perspective that increases spatial frequency along the fence. Aliasing is a prominent artifact in this image. The homogeneity-directed interpolation algorithm reconstructs this image best. Very little aliasing is present in the output image. The “boat” image in Figure 11 contains lines at various angles across the image. This is a good example to show how the algorithms respond to features at various orientations. The POCS algorithm and the homogeneity-directed interpolation algorithm show very few of the aliasing artifacts present in the other output images. This shows that these algorithms are fairly robust to the orientation of various features. According to the MSE measurements, POCS is the best algorithm, but the output

images from the homogeneity-directed method have fewer artifacts. This suggests the need to use subjective evaluations along with objective measures.

In [24], Longere et al. provide a perceptual assessment of demosaicking algorithms. They compare several algorithms with a subjective experiment. The results of their first experiment show that the subjects favored sharpness and the algorithms providing a sharp image were highly favored. The experiment is repeated with the resulting images normalized for sharpness. After this adjustment, the results show more variation and no one algorithm is highly favored. Another comparison of demosaicking algorithms is provided in [29].

CONCLUSIONS AND FUTURE DIRECTIONS

The sensor size of digital cameras continues to decrease, providing sensor

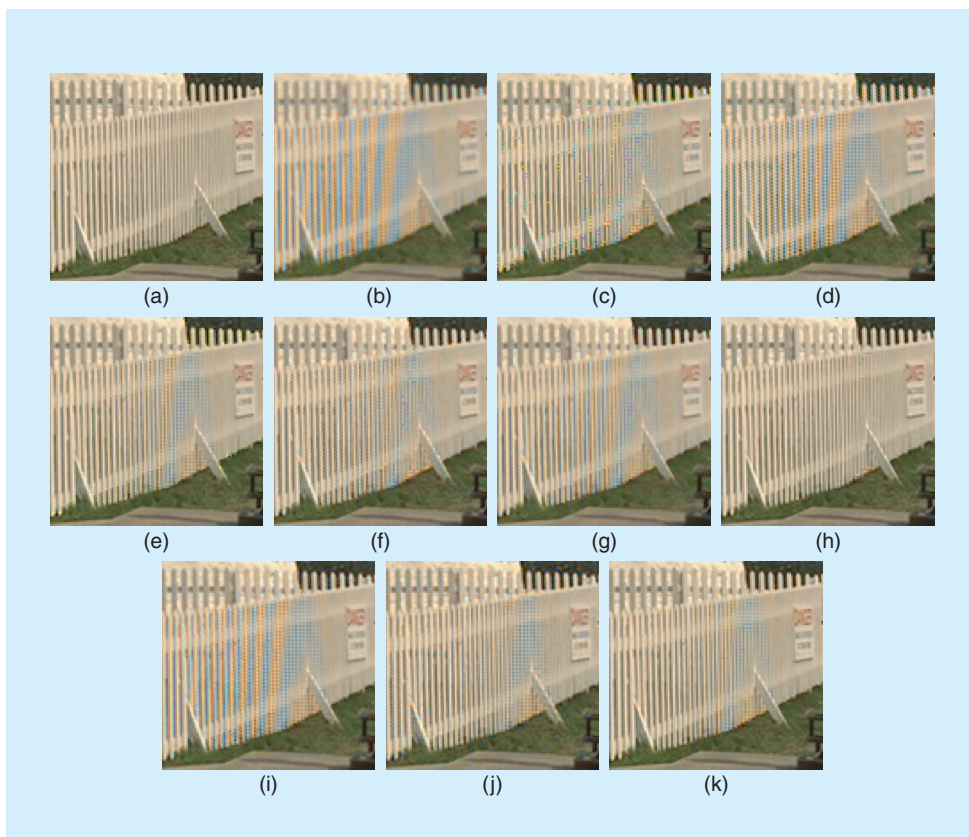


[FIG10] Result images for the “lighthouse” image. (a) Original image. (b) Bilinear interpolation. (c) Edge-directed interpolation in [17]. (d) Constant-hue-based interpolation in [3]. (e) Weighted sum in [22]. (f) Second-order gradients as correction terms in [4]. (g) Bayesian approach in [26]. (h) Homogeneity-directed in [18]. (i) Pattern matching in [8]. (j) Alias cancellation in [12]. (k) POCS in [14].

arrays with larger numbers of pixels. Today, five and six megapixel cameras are common. The increased sampling rate of these cameras reduces the occurrence of aliasing and other artifacts; on the other hand, sensor noise becomes an issue. Recently, Foveon Inc. has invented an imaging sensor, the X3 sensor, that is able to capture R, G, and B information at every pixel; eliminating the need for demosaicking in the digital camera pipeline.

However, research into demosaicking is still an important problem. This research has explored the imaging process and the correlation among three color planes. This extends beyond three color planes into hyperspectral image processing. Another research problem is artifact reduction in color image sequences. Restoration algorithms for image sequences should exploit temporal correlation in addition to spectral correlation. Super-resolution reconstruction is also directly related to the demosaicking problem.

Processing time is often an important measure for algorithms implemented in real-time systems. A photographer needs to be able to take pictures at a fast rate, and the image processing can sometimes limit this. Several cameras, especially the more expensive digital single-lens-reflex (SLR) cameras, provide access to the raw image data captured by the sensor. With this data, the images can be processed at a later time on a computer. In this case, processing time is not critically important. Therefore, algorithms that perform well, but are computationally complex, can still be considered in off-line processing applications.

ACKNOWLEDGMENTS

This work was supported in part by Texas Instruments Leadership University Program, ONR N00014-01-1-0619, and NSF CCR-0113681. The authors would like to thank Dr. Jayanta Mukherjee and Keigo Hirakawa for providing the software of their algorithms and the reviewers for their valuable comments.

AUTHORS

Bahadır K. Gunturk received the B.S. degree in electrical engineering from Bilkent University, Ankara, Turkey, in 1999 and the M.S. and Ph.D. degrees in electrical engineering from

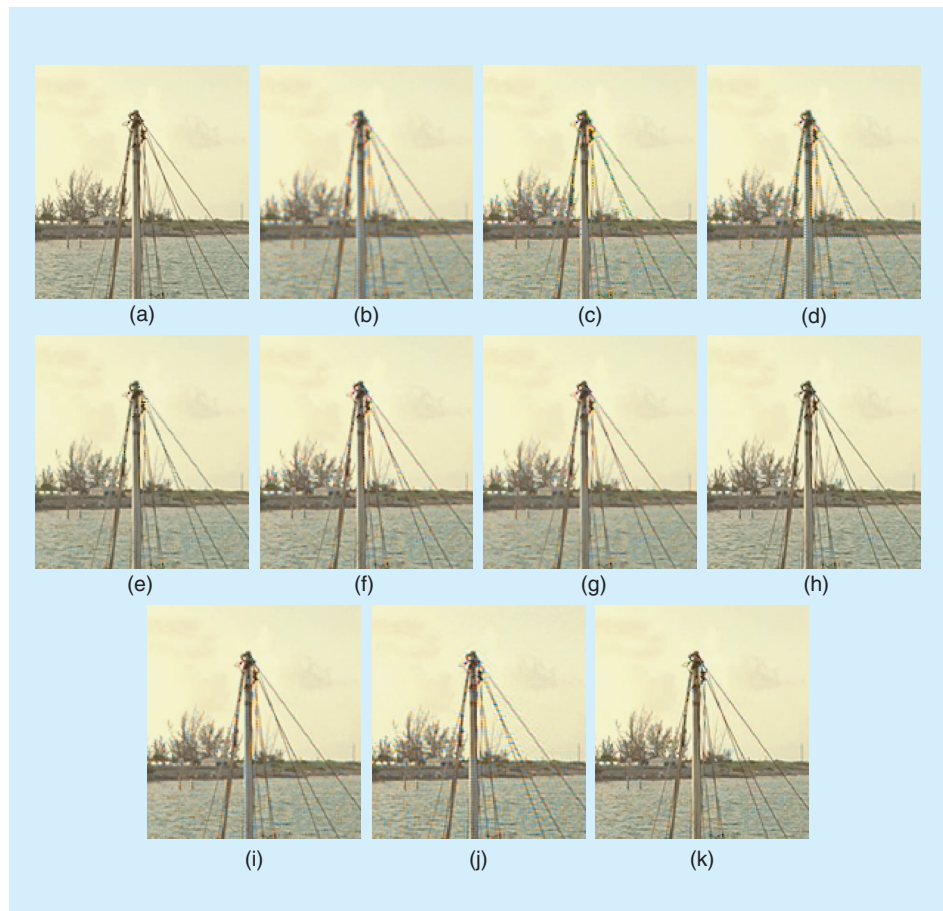


[FIG11] Result images for the “boat” image. (a) Original image. (b) Bilinear interpolation. (c) Edge-directed interpolation in [17]. (d) Constant-hue-based interpolation in [3]. (e) Weighted sum in [22]. (f) Second-order gradients as correction terms in [4]. (g) Bayesian approach in [26]. (h) Homogeneity-directed in [18]. (i) Pattern matching in [8]. (j) Alias cancellation in [12]. (k) POCS in [14].

Georgia Institute of Technology, Atlanta, in 2001 and 2003, respectively. He is currently an assistant professor in the Department of Electrical and Computer Engineering at Louisiana State University. His current research interests are in the areas of image/video processing and computer vision. He received the Outstanding Research Award from the Center for Signal and Image Processing, Georgia Institute of Technology, in 2001. He is a Member of the IEEE.

John Glotzbach received the B.S. degree from Purdue University in 1998 and the M.S. degree in electrical and computer engineering from the Georgia Institute of Technology in 2000. He is currently a Ph.D. student at the Georgia Institute of Technology and a software engineer at Texas Instruments. His research interests include color image processing.

Yucel Altunbasak is an associate professor in the School of Electrical and Computer Engineering at Georgia Institute of Technology. He received the Ph.D. degree from the University of Rochester in 1996. He joined Hewlett-Packard Research Laboratories in July 1996. At that time, he was also a consulting assistant professor at Stanford and San Jose State Universities. He is an associate editor for *IEEE Transactions on Image*

Processing, *IEEE Transactions on Signal Processing*, *Signal Processing: Image Communications*, and the *Journal of Circuits, Systems and Signal Processing*. He is vice-president for the IEEE Communications Society MMC Technical Committee and is a member of the IEEE Signal Processing Society IMDSP Technical Committee. He was cochair for "Advanced Signal Processing for Communications" Symposia at ICC'03. He is the technical program chair for ICIP'06. He received the National Science Foundation (NSF) CAREER Award. He is a recipient of the "2003 Outstanding Junior Faculty Award" at Gatech-ECE, and he is a Senior Member of the IEEE.

Ronald W. Schafer received the B.S.E.E. and M.S.E.E. degrees from the University of Nebraska in 1961 and 1962, respectively, and the Ph.D. degree from MIT in 1968. From 1968 to 1974 he was a member of the Acoustics Research Department, Bell Laboratories, Murray Hill, New Jersey. From 1974 to 2004 he served as John and Marilu McCarty Regents Professor of Electrical and Computer Engineering at the Georgia Institute of Technology. He has coauthored six textbooks, including *Discrete-Time Signal Processing*, *Digital Processing of Speech Signals*, and *Signal Processing First*. He is now a distinguished technologist at Hewlett-Packard Laboratories in Palo Alto, California. He is a Fellow of the IEEE and the Acoustical Society of America and a member of the National Academy of Engineering. He has received numerous awards, including the 1985 Distinguished Professor Award at Georgia Tech and the 1992 IEEE Education Medal.

Russell M. Mersereau received the S.B. and S.M. degrees in 1969 and the Sc.D. in 1973 from MIT. He joined the School of Electrical and Computer Engineering at the Georgia Institute of Technology in 1975. His current research interests are in the development of algorithms for the enhancement, modeling, and coding of computerized images, synthesis aperture radar, and computer vision. He is the coauthor of the text *Multidimensional Digital Signal Processing*. He has served on the editorial board of the *Proceedings of the IEEE* and as associate editor for signal processing of the *IEEE Transactions on Acoustics, Speech, and Signal Processing* and *Signal Processing Letters*. He is received the 1976 IEEE Bowder J. Thompson Memorial Prize, the 1977 Research Unit Award of the Southeastern Section of the ASEE, three teaching awards, and the 1990 Society Award of the IEEE Signal Processing Society. He is currently the vice president for awards and membership of the IEEE Signal Processing Society.

REFERENCES

- [1] B. Wandell, "S-CIELAB: A spatial extension of the CIE L*a*b* DeltaE color difference metric." [Online]. Available: <http://white.stanford.edu/~brian/scielab/scielab.html>
- [2] J. Adams, K. Parulski, and K. Spaulding, "Color processing in digital cameras," *IEEE Micro*, vol. 18, no. 6, pp. 20–31, 1998.
- [3] J.E. Adams, "Interactions between color plane interpolation and other image processing functions in electronic photography," *Proc. SPIE*, vol. 2416, pp. 144–151, 1995.
- [4] J.E. Adams and J.F. Hamilton, "Design of practical color filter array interpolation algorithms for digital cameras," *Proc. SPIE*, vol. 3028, pp. 117–125, 1997.
- [5] D. Alleysson, S. Süssstrunk, and J. Herault, "Color demosaicing by estimating luminance and opponent chromatic signals in the fourier domain," in *Proc. Color Imaging Conf.: Color Science, Systems, Applications*, 2002, pp. 331–336.
- [6] Z. Baharav and R. Kakarala, "Compression aware demosaicing methods," *Proc. SPIE*, vol. 4667, pp. 149–156, 2002.
- [7] D.H. Brainard, "Bayesian method for reconstructing color images from trichromatic samples," in *Proc. IST 47th Annu. Meeting*, 1994, pp. 375–380.
- [8] E. Chang, S. Cheung, and D. Pan, "Color filter array recovery using a threshold-based variable number of gradients," *Proc. SPIE*, vol. 3650, pp. 36–43, 1999.
- [9] D.R. Cok, "Signal processing method and apparatus for producing interpolated chrominance values in a sampled color image signal," U.S. Patent 4 642 678, 1986.
- [10] W.T. Freeman, "Method and apparatus for reconstructing missing color samples," U.S. Patent 4 774 565, 1988.
- [11] S. Geman and D. Geman, "Stochastic relaxation, gibbs distributions and the bayesian distribution of images," *IEEE Trans. Pattern Anal. Machine Intell.*, vol. 6, no. 6, pp. 721–741, 1984.
- [12] J.W. Glotzbach, R.W. Schafer, and K. Illgner, "A method of color filter array interpolation with alias cancellation properties," in *Proc. IEEE Int. Conf. Image Processing*, vol. 1, 2001, pp. 141–144.
- [13] J. Go, K. Sohn, and C. Lee, "Interpolation using neural networks for digital still cameras," *IEEE Trans. Consumer Electron.*, vol. 46, no. 3, pp. 610–616, Aug. 2000.
- [14] B.K. Gunturk, Y. Altunbasak, and R.M. Mersereau, "Color plane interpolation using alternating projections," *IEEE Trans. Image Processing*, vol. 11, no. 9, pp. 997–1013, Sept. 2002.
- [15] M.R. Gupta and T. Chen, "Vector color filter array interpolation," *Proc. SPIE*, vol. 4306, pp. 374–382, 2001.
- [16] Y. Hel-Or and D. Keren, "Image demosaicing method utilizing directional smoothing," U.S. Patent 6 404 918, 2002.
- [17] R.H. Hibbard, "Apparatus and method for adaptively interpolating a full color image utilizing luminance gradients," U.S. Patent 5 382 976, 1995.
- [18] K. Hirakawa and T.W. Parks, "Adaptive homogeneity-directed demosaicing algorithm," in *Proc. IEEE Int. Conf. Image Processing*, vol. 3, pp. 669–672, 2003.
- [19] R. Kakarala and Z. Baharav, "Adaptive demosaicing with the principal vector method," *IEEE Trans. Consumer Electron.*, vol. 48, no. 4, pp. 932–937, Nov. 2002.
- [20] O. Kapah and H.Z. Hel-Or, "Demosaicing using artificial neural networks," *Proc. SPIE*, vol. 3962, pp. 112–120, 2000.
- [21] D. Keren and M. Osadchy, "Restoring subsampled color images," *Mach. Vis. Appl.*, vol. 11, no. 4, pp. 197–202, Dec. 1999.
- [22] R. Kimmel, "Demosaicing: image reconstruction from CCD samples," *IEEE Trans. Image Processing*, vol. 8, no. 9, pp. 1221–1228, 1999.
- [23] C.A. Laroche and M.A. Prescott, "Apparatus and method for adaptively interpolating a full color image utilizing chrominance gradients," U.S. Patent 5 373 322, 1994.
- [24] P. Longere, X. Zhang, P.B. Delahunt, and D.H. Brainard, "Perceptual assessment of demosaicing algorithm performance," *Proc. IEEE*, vol. 90, no. 1, pp. 123–132, Jan. 2002.
- [25] W. Lu and Y.-P. Tan, "Color filter array demosaicing: New method and performance measures," *IEEE Trans. Image Processing*, vol. 12, no. 10, pp. 1194–1210, Oct. 2003.
- [26] J. Mukherjee, R. Parthasarathi, and S. Goyal, "Markov random field processing for color demosaicing," *Pattern Recognit. Lett.*, vol. 22, no. 3–4, pp. 339–351, Mar. 2001.
- [27] S.-C. Pei and I.-K. Tam, "Effective color interpolation in CCD color filter arrays using signal correlation," *IEEE Trans. Circuits Syst. Video Technol.*, vol. 13, no. 6, pp. 503–513, June 2003.
- [28] R. Ramanath and W.E. Snyder, "Adaptive demosaicing," *J. Electron. Imaging*, vol. 12, no. 4, pp. 633–642, Oct. 2003.
- [29] R. Ramanath, W.E. Snyder, G.L. Bilbro, and W.A. Sander III, "Demosaicing methods for Bayer color arrays," *J. Electron. Imaging*, vol. 11, no. 3, pp. 306–315, July 2002.
- [30] B. Tao, I. Tastl, T. Cooper, M. Blasgen, and E. Edwards, "Demosaicing using human visual properties and wavelet interpolation filtering," in *Proc. Color Imaging Conf.: Color Science, Systems, Applications*, 1999, pp. 252–256.
- [31] D. Taubman, "Generalized Wiener reconstruction of images from colour sensor data using a scale invariant prior," in *Proc. IEEE Int. Conf. Image Processing*, vol. 3, 2000, pp. 801–804.
- [32] H.J. Trussell and R.E. Hartwig, "Mathematics for demosaicing," *IEEE Trans. Image Processing*, vol. 3, no. 11, pp. 485–492, Apr. 2002.
- [33] P.-S. Tsai, T. Acharya, and A.K. Ray, "Adaptive fuzzy color interpolation," *J. Electron. Imaging*, vol. 11, no. 3, pp. 293–305, July 2002.
- [34] J.A. Weldy, "Optimized design for a single-sensor color electronic camera system," *Proc. SPIE*, vol. 1071, pp. 300–307, May 1988.
- [35] X. Wu, W.K. Choi, and P. Bao, "Color restoration from digital camera data by pattern matching," *Proc. SPIE*, vol. 3018, pp. 12–17, Apr. 1997.
- [36] X. Zhang and B.A. Wandell, "A spatial extension of CIELAB for digital color image reproduction," in *Soc. Inform. Display Symp. Tech. Dig.*, vol. 27, 1996, pp. 731–734.